Dual Reference Frame Based Current Harmonic Minimization for Dual Three-Phase PMSM Considering Inverter Voltage Limit

Guodong Feng, *Senior Member, IEEE*, Chunyan Lai, *Senior Member, IEEE*, Wenlong Li, *Senior Member, IEEE*, Ze Li, *Graduate Student Member, IEEE*, and Narayan C. Kar, *Senior Member, IEEE*

***Abstract*—This article proposes an optimized current harmonic minimization (CHM) approach for dual three-phase permanent magnet synchronous machines (PMSMs) with consideration of inverter voltage limit. The current harmonic model is derived to analyze the dominant current harmonic components in dual three-phase PMSM drives. Dual reference frame (DRF) model is proposed to convert the current harmonics into dc components in the new DRFs, and PI controllers are employed to control voltages to minimize the dc components. This article will prove that current harmonics can be minimized by using the DRF model. Since CHM requires additional voltages, inverter voltage limit must be considered especially at high speeds. Hence, inverter voltage limit is considered to derive the theoretical control strategy, in which minimal copper loss is selected as the design objective to reduce current harmonic with limited voltage. The proposed approach is supported by theoretical analysis and proof, and it does not require inverter voltage and machine parameters. Moreover, the proposed approach is compared with an existing method to show the performance improvement and evaluated with extensive tests on a laboratory prototype under both steady-state and transient conditions.**

***Index Terms*—Current harmonic minimization (CHM), dual reference frame (DRF), dual three-phase permanent magnet synchronous machine (PMSM), inverter voltage limit.**

I. Introduction

IN COMPARISON to the conventional three-phase permanent magnet synchronous machines (PMSMs), multiphase PMSMs are better in terms of fault-tolerant capability and reducing the per phase power rating [1]–[4]. The dual three-phase PMSM is a popular multiphase PMSM configuration received much research interests for industrial applications, such as electric vehicles. In a dual three-phase PMSM drive, current harmonics are inevitable due to the nonlinearities of the machine and drive [5], [6]. Current harmonics will be even severer at high-speed region or for high-speed machines [7]. On the other hand, current harmonics can cause additional machine losses, torque ripples, and vibrations [8], [9] resulting in reduced efficiency and performance. Therefore, this article investigates current harmonic minimization (CHM) of dual three-phase PMSM for high-performance and efficient control.

In the drive system, dual three-phase PMSMs are driven by a multiphase voltage source inverter, and the motor control is based on the inputs, including current, position, and/or voltage measurements. The inverter nonlinearity will introduce voltage harmonics and thus current harmonics, and the measurement errors can also induce current harmonics [10]–[16]. Moreover, PM flux linkage harmonics are existing in the machine, and there are also voltage harmonics due to pulsewidth modulation [17], [18]. All of these will contribute to the current harmonics in the machine.

In the literature, CHM has been widely investigated for PMSMs, and the approaches can be divided into mainly two categories, namely, the model-based approach and the model-free approach. In the first approach, high-frequency (HF) model is employed to calculate the compensating voltage harmonics [7], which produces opposite current harmonics to cancel the existing ones. For instance, in [19], current harmonics due to inverter deadtime are modeled and compensated for the dual three-phase PMSM. However, current harmonics are caused by multiple sources with uncertainties, so it is challenging to accurately model and minimize all the harmonics. Moreover, model-based approach requires accurate parameters, such as resistance and inductance, which are not available in the motor drive. These parameters can also change during machine operation [20]. Therefore, it is challenging to ensure the performance of the model-based approach. In the second approach, harmonics extracted from current measurements are used as the feedback control inputs to control voltage harmonics to

Manuscript received April 10, 2020; revised July 8, 2020 and October 7, 2020; accepted November 19, 2020. Date of publication December 1, 2020; date of current version March 5, 2021. This work was supported in part by the Key-Area Research and Development Program of Guangdong Province under Grant 2020B090920002 and in part by the Fundamental Research Funds for the Central Universities under Grant 20LGPY18. Recommended for publication by Associate Editor J. He. *(Corresponding author: Guodong Feng.)*

Guodong Feng is with the School of Intelligent Systems Engineering, Sun Yat-sen University, Guangzhou 510006, China (e-mail: fenggd6@mail.sysu.edu.cn).

Chunyan Lai is with the Department of Electrical and Computer Engineering, Concordia University, Montreal, QC H3G 1M8, Canada (e-mail: chunyan.lai@concordia.ca).

Wenlong Li, Ze Li, and Narayan C. Kar are with the Department of Electrical and Computer Engineering, University of Windsor, Windsor, ON N9B 3P4, Canada (e-mail: wenlong.li@uwindsor.ca; li111169@uwindsor.ca; nkar@uwindsor.ca).

Color versions of one or more figures in this article are available at https://doi.org/10.1109/TPEL.2020.3041749.

Digital Object Identifier 10.1109/TPEL.2020.3041749

be injected for CHM. For instance, in [21], [22], proportional resonant (PR) controller is employed to minimize the current harmonics. However, PR coefficients should be optimized for different harmonic orders [23], [24], which impose complexity to the control design for CHM under various speed conditions. In addition to aforementioned approaches, there are also existing research works on improving the motor controllers to reduce current harmonics. In [25]–[27], optimized reference voltage vectors are developed to reduce the current harmonics for model predictive or direct torque controllers, which, however, do not consider the dominant current harmonics due to the flux harmonics and inverter distortion. In [28], open-end motor configuration with zero-axis current control is proposed for current harmonic suppression, which, however, requires doubled power switches in the inverter, thus increases the cost and limits the applicability. In [29], leaning algorithm is employed to develop feedforward voltage compensation to minimize the current harmonics, which involves offline training procedure.

For dual three-phase PMSMs, vector space decomposition (VSD) model is widely employed for modeling and control, in which there are two DQ frames, namely, DQ_1 and DQ_2, and only DQ_1 frame contributes to torque production. However, DQ_2 frame inductances are significantly smaller than DQ_1 frame inductances [30]–[32], thus DQ_2 frame impedances are much smaller than that of DQ_1 frame for the same harmonic order. Hence, current harmonics are more significant in DQ_2 frame due to the lower impedances. Moreover, the dominant current harmonic occupies most of the harmonics in both DQ_1 and DQ_2 frames, so it is critical to minimize these harmonics. However, existing approaches for three-phase PMSM are unable to deal with DQ_1 and DQ_2 frame current harmonics of dual three-phase PMSMs simultaneously due to the distinctions in the model and machine properties.

Moreover, CHM involves voltage harmonics injection. Due to inverter voltage limit, there could be not enough voltage for CHM especially at high-speed region [33], [34]. However, inverter voltage limit has not been fully addressed in the literature for current harmonic reduction.

This article proposes a novel CHM approach for the dual three-phase PMSM, in which the inverter voltage limit is considered. First, the current harmonic model is developed to analyze the harmonic components, which will show that there are dominant 12th harmonic in the DQ_1 frame and 6th harmonic in the DQ_2 frame. This article proposes a dual reference frame (DRF) model for CHM in the synchronous frame, which will not affect the dc current control for torque production. This article will prove that the proposed approach is able to minimize the current harmonics to zero. Moreover, when the constraint of inverter voltage limit is imposed, the proposed approach can reduce the current harmonics with minimal copper loss. The theoretical analysis and proof are provided to support the proposed approach. Compared with existing methods, the proposed approach does not require inverter voltage and machine parameters, and it can also ensure minimal copper loss induced by the current harmonics. The proposed approach is validated with extensive experiments and comparisons with an existing method on a laboratory machine under various operating conditions.

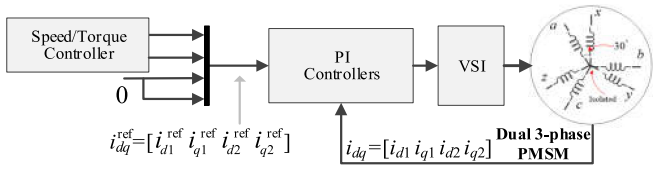

Fig. 1. VSD model based dual three-phase PMSM control.

II. Modeling and Analysis of the Current Harmonics in a Dual Three-Phase PMSM Drive

The dual three-phase PMSM under investigation is shown in Fig. 1, in which the two sets of three-phase windings consist of a phase shift of $\pi/6$ and have isolated neutral points. The VSD-based model can be denoted as

$$\begin{cases} u_{d1} = Ri_{d1} + L_{d1}\frac{di_{d1}}{dt} - \omega L_{q1} i_{q1} \\ u_{d2} = Ri_{d2} + L_{d2}\frac{di_{d2}}{dt} - \omega L_{q2} i_{q2} \\ u_{q1} = Ri_{q1} + L_{q1}\frac{di_{q1}}{dt} + \omega L_{d1} i_{d1} + \omega \lambda_0 \\ u_{q2} = Ri_{q2} + L_{q2}\frac{di_{q2}}{dt} + \omega L_{d2} i_{d2} \end{cases} \tag{1}$$

$$t_e = 3P\left(\lambda_0 i_{q1} + (L_{d1} - L_{q1}) i_{d1} i_{q1}\right) \tag{2}$$

where u_{dk}, u_{qk}, i_{dk}, i_{qk}, L_{dk} and L_{qk}, respectively, denote the DQ_k axis voltages, currents, and inductances in VSD model, $k = 1$ or 2, ω is the rotor electrical speed; λ_0 is the PM flux linkage, t_e is the output torque; and P is the number of pole pairs. This model assumes that the back electromotive force is sinusoidal; eddy current and hysteresis losses, mutual leakage inductance, and the harmonics in self and mutual inductances with orders higher than two are neglected [30]. In this model, t_e is a function of DQ_1 frame currents and the discussion of the inductances is presented in the Appendix.

Fig. 1 presents VSD-based motor control, where i_{d2} and i_{q2} are controlled to zero while the references ${i_{d1}}^{\text{ref}}$ and ${i_{q1}}^{\text{ref}}$ are obtained from the outer loop controller. The transformation matrix $\mathrm{T_{DQ}}$ in [5] is utilized to convert the six-phase currents into DQ frame currents $i_{dq} = [i_{d1}\ i_{q1}\ i_{d2}\ i_{q2}]^{\mathrm{T}}$ and the PI controllers control the actual currents to follow their references.

Fig. 2 presents the DQ frame currents of the test motor running at 200 r/min. The parameters of the test motor will be given in Section IV. Ideally, i_{d1} and i_{q1} should contain only dc components for torque production; i_{d2} and i_{q2} should be zero as they have no contribution to torque production. However, due to reasons, such as inverter distortion, currents harmonics are inevitable. As shown in Fig. 2, there are 12th and 24th harmonics in i_{d1} and i_{q1}; and 6th and 18th harmonics in i_{d2} and i_{q2}. The reason why i_{d2} and i_{q2} have more significant harmonics will be explained by the current harmonic model at the end of this section. Moreover, the most dominant harmonic occupies most of the total harmonics. Therefore, it is necessary to minimize the most dominant harmonic in DQ frame currents.

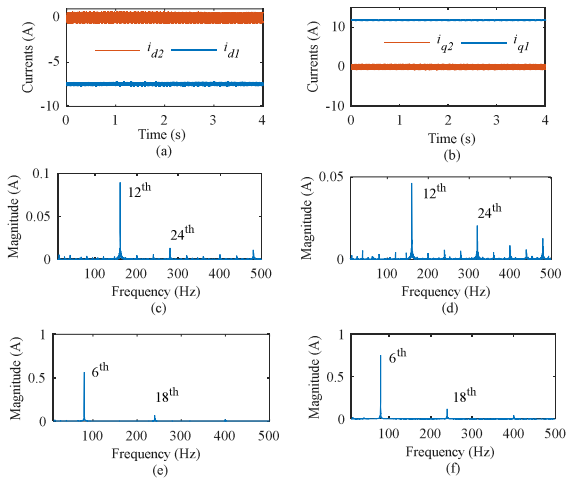

Fig. 2. DQ frame currents of the test machine. (a) D_1D_2 frame currents. (b) Q_1Q_2 frame currents. Harmonic components of (c) i_{d1}, (d) i_{q1}, (e) i_{d2}, and (f) i_{q2}. The dc components of DQ frame currents are not presented in (c)–(f).

To model the current harmonics, DQ frame currents are represented as

$$\begin{cases} i_{d1} = I_{d0} + \sum_k i_{dk} = I_{d0} + \sum_k I_{dk}\cos(k\theta - \phi_{dk}) \\ i_{q1} = I_{q0} + \sum_k i_{qk} = I_{q0} + \sum_k I_{qk}\sin(k\theta - \phi_{qk}) \\ i_{d2} = \sum_l i_{dl} = \sum_l I_{dl}\cos(l\theta - \phi_{dl}) \\ i_{q2} = \sum_l i_{ql} = \sum_l I_{ql}\sin(l\theta - \phi_{ql}) \end{cases} \tag{3}$$

where I_{d0} and I_{q0} are the dc components of i_{d1} and i_{q1}, respectively; i_{dk}, i_{qk}, i_{dl}, and i_{ql} are the harmonic components of i_{d1}, i_{q1}, i_{d2}, and i_{q2}, respectively; I_{dk} and I_{qk} are the magnitudes of i_{dk} and i_{qk}, respectively, and ϕ_{dk} and ϕ_{qk} are the phase angles; I_{dl} and I_{ql} are the magnitudes of i_{dl} and i_{ql}, respectively; and ϕ_{dl} and ϕ_{ql} are the phase angles.

The harmonic components in (3) will cause torque ripples and additional losses. According to the torque model in [6], the torque ripple will increase as the increase of current harmonics. Moreover, machine losses induced by the current harmonics increase with the increase of current harmonics. Therefore, it is necessary to minimize the dominant current harmonics to avoid the resulted adverse effects.

In the dual three-phase PMSM drive, the current harmonics are mainly induced by the inverter distortion and the PM flux linkage harmonics. The inverter distortion will produce the kth voltage harmonics in DQ_1 frame and lth voltage harmonics in DQ_2 frame ($k = 12, 24, 36\ldots$, and $l = 6, 18, 30\ldots$). Moreover, for PM flux linkages, there are kth harmonic in DQ_1 frame and lth harmonic in DQ_2 frame. These harmonics produce the current harmonics in DQ frame.

Suppose that the total voltage harmonics in DQ_1 and DQ_2 frames are represented as

$$\begin{cases} v_{d1,h} = \sum_k v_{dk} = \sum_k V_{dk}\cos(k\theta - \varphi_{dk}) \\ v_{q1,h} = \sum_k v_{qk} = \sum_k V_{qk}\sin(k\theta - \varphi_{qk}) \\ v_{d2,h} = \sum_l v_{dl} = \sum_l V_{dl}\cos(l\theta - \varphi_{dl}) \\ v_{q2,h} = \sum_l v_{ql} = \sum_l V_{ql}\sin(l\theta - \varphi_{ql}) \end{cases} \tag{4}$$

where $v_{d1,h}$, $v_{q1,h}$, $v_{d2,h}$, and $v_{q2,h}$ denote the voltage harmonics; V_{dk} and V_{qk} are the magnitudes of the kth harmonics in DQ_1 frame, and φ_{dk} and φ_{qk} are the phase angles; V_{dl} and V_{ql} are the magnitudes of the lth harmonics in DQ_2 frame, and φ_{dl} and φ_{ql} are the phase angles.

This article aims to minimize the current harmonics, so the HF model is employed and according to Reigosa *et al.* [35] and Reigosa *et al.* [36], the HF model of a dual three-phase PMSM can be derived as

$$\begin{cases} u_{d1,h} = R_{d1h}i_{d1,h} + L_{d1}\frac{di_{d1,h}}{dt} \\ u_{q1,h} = R_{q1h}i_{q1,h} + L_{q1}\frac{di_{q1,h}}{dt} \\ u_{d2,h} = R_{d2h}i_{d2,h} + L_{d2}\frac{di_{d2,h}}{dt} \\ u_{q2,h} = R_{q2h}i_{q2,h} + L_{q2}\frac{di_{q2,h}}{dt} \end{cases} \tag{5}$$

where the subscript "$_h$" represents the HF components or HF machine parameters, which hold throughout this article.

Based on (3)–(5), the current harmonics can be modeled by using the voltage harmonics and the HF impedances as

$$\begin{aligned} &i_{dk} = \frac{v_{dk}}{Z_{dk}},\ i_{qk} = \frac{v_{qk}}{Z_{qk}},\ i_{dl} = \frac{v_{dl}}{Z_{dl}},\ i_{ql} = \frac{v_{ql}}{Z_{ql}} \\ &\text{with} \begin{cases} Z_{dk} = R_{dk} + j\omega_k L_{dk}, & Z_{qk} = R_{qk} + j\omega_k L_{qk} \\ Z_{dl} = R_{dl} + j\omega_l L_{dl}, & Z_{ql} = R_{ql} + j\omega_l L_{ql} \end{cases} \end{aligned} \tag{6}$$

where Z_{dk} is the HF impendence at the frequency of the kth harmonic; R_{dk} is the HF resistance, and L_{dk} is the HF inductance in D_1 axis; and similar for Z_{qk}, Z_{dl}, and Z_{ql}; and $\omega_{k/l} = 2\pi f_{k/l}$ with $f_{k/l}$ being the frequency of the kth or lth harmonic.

It can be concluded from (6) that one can compensate the voltage harmonics to produce extra current harmonics to cancel existing ones. However, obtaining the required voltage harmonics involves the HF resistances and inductances, which are not always available. Therefore, it is challenging to use (6) for CHM. On the other hand, the inductances in DQ_2 frame are leakage inductances [30], which are much smaller than the inductances in DQ_1 frame. This conclusion can also be found in [37]. According to (6), for the same harmonic order, the HF impendences in DQ_2 frame are much smaller than that in DQ_1 frame. This is the reason why the 6th current harmonic in DQ_2 frame has a much larger magnitude than the 12th current harmonic in DQ_1 frame, as shown in Fig. 2. Moreover, this conclusion is also valid in other references, such as [7]. Next section will present CHM considering inverter voltage limit.

III. DRF-Based CHM Considering Inverter Voltage Limit

The schematic diagram of the proposed DRF-based CHM is shown in Fig. 3. The objective is to minimize the harmonic components in DQ_1 and DQ_2 frame currents. In Fig. 3, when there is no inverter voltage limit, the references $I_1^{\text{ref}}, \ldots, I_8^{\text{ref}}$ will be set to zero to minimize current harmonics to zero; when inverter voltage is limited, $I_1^{\text{ref}}, \ldots, I_8^{\text{ref}}$ will be optimized to reduce the current harmonics. This section first presents DRF-based model and then considers the inverter voltage limit. Current harmonics with different orders are independent of each other, so each harmonic order can be minimized independently. Moreover, the most dominant harmonics in DQ_1 and DQ_2 occupy most of

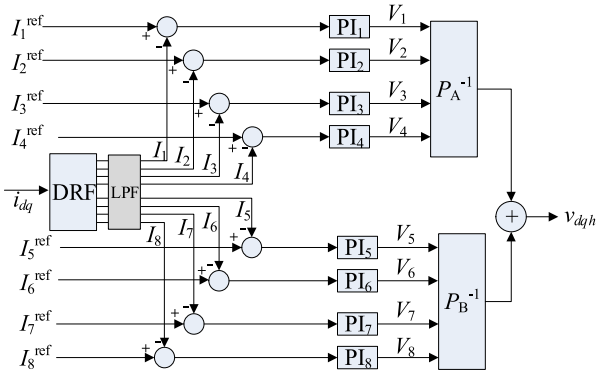

Fig. 3. DRF-based CHM control, where references $I_1{}^{\text{ref}},\ldots,I_8{}^{\text{ref}}$ will be set to zero for CHM without inverter voltage limit; $I_1{}^{\text{ref}},\ldots,I_8{}^{\text{ref}}$ will be optimized for current harmonic reduction with inverter voltage limit.

the harmonics. Hence, this article specifically minimizes the *k*th current harmonic as the most dominant one in DQ_1 frame and the *l*th current harmonic as the most dominant one in DQ_2 frame for demonstration.

A. DRF-Based CHM

In Fig. 3, this article aims to minimize the current harmonics in the synchronous frame. The idea is to project *k*th and *l*th current harmonics in the synchronous frame into DRFs at the same frequencies of the current harmonics. In this way, *k*th and *l*th harmonics in the synchronous frame become dc components in DRFs, so CHM in the synchronous frame is equivalent to minimizing dc components in the DRFs and PI controller is capable of achieving this task. The proposed approach is able to minimize the *k*th and *l*th current harmonics under both transient and steady-state conditions. Moreover, the proposed approach will not affect the control of dc currents in DQ frame. Specifically, the proposed approach consists of following three steps.

Step 1: The first step is to project the *k*th and *l*th harmonic components into the dc components using DRFs. To this end, the DRF transformations P_{A} and P_{B} are defined as in (7) and their inverses are defined as in (8)

$$P_A = \begin{bmatrix} P_1(k) & \mathbf{0}_{2\times 2} \\ \mathbf{0}_{2\times 2} & P_1(l) \end{bmatrix},\ P_B = \begin{bmatrix} P_2(k) & \mathbf{0}_{2\times 2} \\ \mathbf{0}_{2\times 2} & P_2(l) \end{bmatrix}$$

with

$$P_1(k) = \begin{bmatrix} \cos k\theta & -\sin k\theta \\ \sin k\theta & \cos k\theta \end{bmatrix}$$

$$P_2(k) = \begin{bmatrix} \cos k\theta & \sin k\theta \\ -\sin k\theta & \cos k\theta \end{bmatrix} \tag{7}$$

$$P_A^{-1} = P_A^{\text{T}},\ P_B^{-1} = P_B^{\text{T}} \tag{8}$$

where *k*/*l* denotes the order of the current harmonic in $\text{DQ}_{1/2}$ frame; *k* and *l* can be either equal or unequal to each other depending on the current harmonics in DQ_1 and DQ_2 frames to be minimized. In (7), P_A and P_B are 4×4 matrices.

Multiplying the current harmonics (*k*th at DQ_1 frame and *l*th at DQ_2 frame) in the synchronous frame with P_A and P_B in (7), the results are

$$\begin{bmatrix} P_A \\ P_B \end{bmatrix} \begin{bmatrix} i_{dk} \\ i_{qk} \\ i_{dl} \\ i_{ql} \end{bmatrix}$$

$$= \begin{bmatrix} I_{dk}\cos k\theta\cos(k\theta-\phi_{dk}) - I_{qk}\sin k\theta\cos(k\theta-\phi_{qk}) \\ I_{dk}\sin k\theta\cos(k\theta-\phi_{dk}) + I_{qk}\cos k\theta\cos(k\theta-\phi_{qk}) \\ I_{dl}\cos l\theta\cos(l\theta-\phi_{dl}) - I_{ql}\sin l\theta\cos(l\theta-\phi_{ql}) \\ I_{dl}\sin l\theta\cos(l\theta-\phi_{dl}) + I_{ql}\cos l\theta\cos(l\theta-\phi_{ql}) \\ I_{dk}\cos k\theta\cos(k\theta-\phi_{dk}) + I_{qk}\sin k\theta\cos(k\theta-\phi_{qk}) \\ -I_{dk}\sin k\theta\cos(k\theta-\phi_{dk}) + I_{qk}\cos k\theta\cos(k\theta-\phi_{qk}) \\ I_{dl}\cos l\theta\cos(l\theta-\phi_{dl}) + I_{ql}\sin l\theta\cos(k\theta-\phi_{ql}) \\ -I_{dl}\sin l\theta\cos(l\theta-\phi_{dl}) + I_{ql}\cos l\theta\cos(k\theta-\phi_{ql}) \end{bmatrix}. \tag{9}$$

In (9), there are both dc and harmonic components. In order to obtain the dc values in the DRFs, low-pass filter (LPF) is applied to (9), and the results are

$$\text{LPF}\left(\begin{bmatrix} P_A \\ P_B \end{bmatrix} \begin{bmatrix} i_{dk} \\ i_{qk} \\ i_{dl} \\ i_{ql} \end{bmatrix}\right)$$

$$= \frac{1}{2}\begin{bmatrix} I_{dk}\cos\phi_{dk} - I_{qk}\sin\phi_{qk} \\ I_{dk}\sin\phi_{dk} + I_{qk}\cos\phi_{qk} \\ I_{dl}\cos\phi_{dl} - I_{ql}\sin\phi_{ql} \\ I_{dl}\sin\phi_{dl} + I_{ql}\cos\phi_{ql} \\ I_{dk}\cos\phi_{dk} + I_{qk}\sin\phi_{qk} \\ -I_{dk}\sin\phi_{dk} + I_{qk}\cos\phi_{qk} \\ I_{dl}\cos\phi_{dl} + I_{ql}\sin\phi_{ql} \\ -I_{dl}\sin\phi_{dl} + I_{ql}\cos\phi_{ql} \end{bmatrix} \triangleq \begin{bmatrix} I_1 \\ I_2 \\ I_3 \\ I_4 \\ I_5 \\ I_6 \\ I_7 \\ I_8 \end{bmatrix}. \tag{10}$$

Here, LPF can be a second-order LPF with transfer function *H*(*s*) as

$$H(s) = \frac{\omega_n^2}{s^2 + 2\zeta\omega_n s + \omega_n^2} \tag{11}$$

where *s* is the Laplace operator, $\omega_n = 2\pi f_n$ is the cutoff frequency, and ξ is the damping ratio. In the test, f_n is experimentally set to 5 Hz and ξ is set to 0.707.

As shown in (10), the current harmonics in the synchronous frame are transformed into the dc components $I_1,\ldots,I_8$, where I_k ($k = 1,2,5,6$) corresponds to the *k*th harmonic in DQ_1 frame and I_k ($k = 3,4,7,8$) corresponds to the *l*th harmonic in DQ_2 frame.

Theorem 1: When $I_1,\ldots,I_8$ in DRFs are controlled to zero, I_{dk}, I_{qk}, I_{dl}, and I_{ql} will be zero and, thus, the *k*th and *l*th current harmonics in the synchronous frame are minimized to zero.

Proof to Theorem 1: See the Appendix.

Theorem 1 indicates that the CHM becomes dc component minimization in the DRF, so PI controller can achieve this task.

Step 2: The second step is to use the PI controllers to control $I_1,\ldots,I_8$ to zero. Based on Theorem 1, when $I_1,\ldots,I_8$ are controlled to zero, I_{dk}, I_{qk}, I_{dl}, and I_{ql} will be zero and, thus, the current harmonics are minimized to zero.

As shown in Fig. 3, eight PI controllers are employed to control $I_1,\ldots,I_8$ to zero, and the references ${I_1}^{\text{ref}},\ldots,{I_8}^{\text{ref}}$ are set to zero and the feedback control signals are obtained from the DQ frame currents. The PI controller outputs are the harmonic voltages to be added to reference voltages in the synchronous frame to minimize the current harmonics. The output of the ith PI controller is

$$V_i = K_{P,i}\left(I_i^{\text{ref}} - I_i\right) + K_{I,i}\int\left(I_i^{\text{ref}} - I_i\right)\mathrm{d}t,\ i = 1,\ldots,8 \tag{12}$$

where $K_{P,i}$ and $K_{I,i}$ are the ith PI control gains, and the feedback control signals $I_1,\ldots,I_8$ are calculated from DQ frame currents using (13). The PI coefficients should be properly designed in order to ensure the control performance. Here, PI coefficients are designed according to the proposed model. It is a linear model, so the PI coefficients can be directly calculated from the model coefficients

$$\text{LPF}(P_{A\text{ or }B}[i_{d1}\ i_{q1}\ i_{d2}\ i_{q2}]^T) = \text{LPF}(P_{A\text{ or }B}[i_{dk}\ i_{qk}\ i_{dl}\ i_{ql}]^T). \tag{13}$$

Step 3 The third step is to apply the voltage harmonics to DQ frames. The harmonic voltages to be added to DQ frames in the synchronous frame can be obtained by applying (8) to the dc voltages $V_1,\ldots,V_8$ in (12), which are

$$\begin{aligned}[v_{dk}v_{qk}v_{dl}v_{ql}]^{\mathrm{T}} &= P_A^{-1}[V_1\,V_2\,V_3\,V_4]^{\mathrm{T}} \\ &\quad + P_B^{-1}[V_5\,V_6\,V_7\,V_8]^{\mathrm{T}} \\ &= \begin{bmatrix} V_1\cos k\theta + V_2\sin k\theta + V_5\cos k\theta - V_6\sin k\theta \\ -V_1\sin k\theta + V_2\cos k\theta + V_5\sin k\theta + V_6\cos k\theta \\ V_3\cos l\theta + V_4\sin l\theta + V_7\cos l\theta - V_8\sin l\theta \\ -V_3\sin l\theta + V_4\cos l\theta + V_7\sin l\theta + V_8\cos l\theta \end{bmatrix}.\end{aligned} \tag{14}$$

When there is no inverter voltage limit, the current harmonics can be minimized by setting ${I_1}^{\text{ref}}$ to ${I_8}^{\text{ref}}$ to zero. In this way, the CHM is achieved.

B. With Consideration of Inverter Voltage Limit

This section discusses the inverter voltage limit. During CHM, the voltage harmonics in (14) will be added to DQ frame reference voltages, and the total reference voltages can be denoted as

$$[v_{d1,a}v_{q1,a}v_{d2,a}v_{q2,a}]^{\mathrm{T}} = [v_{d1}v_{q1}v_{d2}v_{q2}]^{\mathrm{T}} + [v_{dk}v_{qk}v_{dl}v_{ql}]^{\mathrm{T}} \tag{15}$$

where $v_{d1,a}$ and v_{d1} represent, respectively, the actual reference voltage and the voltage without CHM in D_1 axis; and similar for $v_{q1,a}$, v_{qk}, $v_{d2,a}$, v_{dl}, $v_{q2,a}$, and v_{ql}.

In $\alpha\beta$-frame, inverter voltage limit can be denoted as [33]

$$v_{\text{limit}} \le \frac{2}{3}U_{\text{dc}} \tag{16}$$

where U_{dc} is dc-link voltage and v_{limit} is not constant.

During CHM, voltage harmonics (14) could result in the total voltage exceeding the voltage limit (16), which can happen especially at high-speed conditions. Hence, it is necessary to consider the inverter voltage limit in CHM.

In order to minimize i_{dk}, i_{qk}, i_{dl}, and i_{ql}, one needs to add the voltage harmonics to generate $-i_{dk}$, $-i_{qk}$, $-i_{dl}$, and $-i_{ql}$ to cancel the existing ones. Based on (6), when (17) is added to the reference voltages, the current harmonics can be minimized

$$[v_{dk}\ v_{qk}\,v_{dl}\ v_{ql}]^T = [-i_{dk}Z_{dk}\ -i_{qk}Z_{qk}\ -i_{dl}Z_{dl}\ -i_{ql}Z_{ql}]^T. \tag{17}$$

When (17) is added to DQ frames, the peak voltage will change accordingly. If inverter voltage is limited, it is unable to provide all the voltages to minimize the current harmonics and one can only reduce the current harmonics to a certain amount. In other words, with limited inverter voltage, the references in Fig. 3 cannot be zero and instead should be optimized.

Taking the test motor as an example, the 6th harmonic in DQ_2 frame has significantly larger magnitude than the 12th harmonic in DQ_1 frame, as shown in Fig. 2. As analyzed in Section II, for the same harmonic order, the impedances in DQ_2 frame are much smaller than that in DQ_1 frame. Hence, with limited voltage, one should minimize the current harmonic in DQ_2 frame with larger magnitude at first. In this way, one can reduce more current harmonics. In other words, with limited voltage, the optimal solution is to suppress the 6th harmonic in DQ_2 frame at first and then suppress the 12th harmonic in DQ_1 frame if the voltage is still available. Without loss of generality, this article focuses on reducing the lth harmonic in DQ_2 frame with limited voltage.

Problem statement: Assume that initially the current harmonics in DQ_2 frames are $i_{dl,0}$ and $i_{ql,0}$, respectively, and they can be, respectively, reduced to $\alpha_1 i_{dl,0}$ and $\alpha_2 i_{ql,0}$ due to limited inverter voltage (without limit α_1 and α_2 will be zero). Since the inverter voltage is limited to reduce the DQ_2 frame current harmonics, the 1st, 2nd, 5th, and 6th PI controllers for DQ_1 frame in Fig. 3 are disabled. The task here is to find optimal α_1 and α_2 satisfying the constraints of inverter voltage limit and machine loss.

According to (6), the voltages required to reduce DQ_2 frame current harmonics to $\alpha_1 i_{dl,0}$ and $\alpha_2 i_{ql,0}$ can be denoted as

$$[\,v_{dl}\ v_{ql}]^T = -[(1-\alpha_1)\ i_{dl,0}Z_{dl}\ \ (1-\alpha_2)\,i_{ql,0}Z_{ql}]^T. \tag{18}$$

Assume that the inverter voltage is limited to V_0, that is

$$|v_{dl}| + |v_{ql}| \le V_0. \tag{19}$$

In fact, one can also consider sqrt($v_{dl}{}^2+v_{ql}{}^2$)$\le V_0$. The major objective is to find α_1 and α_2 satisfying (19).

On the other hand, the induced copper loss is proportional to the square of the magnitudes of current harmonics, therefore, the other objective is to minimize the square of the current magnitudes for loss minimization, that is

$$\min\left(\alpha_1^2 I_{dl,0}^2 + \alpha_2^2 I_{ql,0}^2\right)\ \text{s.t.}\ |v_{dl}| + |v_{ql}| \le V_0 \tag{20}$$

where $I_{dl,0}$ and $I_{ql,0}$ are the magnitudes of $i_{dl,0}$ and $i_{ql,0}$, respectively.

In order to find optimal α_1 and α_2, we construct the Lagrange cost function (21) based on (18) and (20)

$$f(\alpha_1,\alpha_2,\gamma)=\alpha_1^2 I_{dl,0}^2+\alpha_2^2 I_{ql,0}^2 +\gamma\left(\left(1-\alpha_1\right) I_{dl,0}Z_{dl}+\left(1-\alpha_2\right) I_{ql,0}Z_{ql}-V_0\right) \tag{21}$$

where γ denotes the Lagrange coefficient.

To solve (21), we need to compute the partial derivatives as

$$\frac{\partial f}{\partial \alpha_1}=\frac{\partial f}{\partial \alpha_2}=\frac{\partial f}{\partial \gamma} =0\Rightarrow\begin{cases}2\alpha_1 I_{dl,0}^2-\gamma I_{dl,0}Z_{dl}=0\\ 2\alpha_2 I_{ql,0}^2-\gamma I_{ql,0}Z_{ql}=0\\ \left(1-\alpha_1\right)\tau Z_{dl}+\left(1-\alpha_2\right)Z_{ql}=Z_0\end{cases} \tag{22}$$

where $\tau=I_{dl,0}/I_{ql,0}$ and $Z_0=V_0/I_{ql,0}$. By solving (22), optimal α_1 and α_2 can be obtained as

$$\alpha_{1,\mathrm{opt}}=\frac{\tau Z_{dl}+Z_{ql}-Z_0}{\tau\left(Z_{dl}^2+Z_{ql}^2\right)}Z_{dl}\ \alpha_{2,\mathrm{opt}}=\frac{\tau Z_{dl}+Z_{ql}-Z_0}{\left(Z_{dl}^2+Z_{ql}^2\right)}Z_{ql}. \tag{23}$$

Under inverter voltage limit, optimal α_1 and α_2 are theoretically derived in (23). However, voltage limit is unknown and machine parameters can vary. Therefore, it is challenging to use (23) to find the optimal values. To this end, this article explores the relationship between $\alpha_{1,\mathrm{opt}}$ and $\alpha_{2,\mathrm{opt}}$ given in (24) for current harmonic suppression, which is obtained from (23)

$$\frac{\alpha_{1,\mathrm{opt}}}{\alpha_{2,\mathrm{opt}}}=\frac{Z_{dl}}{\tau Z_{ql}}. \tag{24}$$

As discussed in the Appendix, the DQ_2 frame inductances satisfy $L_{d2}=L_{q2}=L_{sl}$. Since resistance and inductance in D_2 frame are equal to that in Q_2 frame, it is reasonable to assume that the impedances in DQ_2 frame are equal, that is, $Z_{dl}=Z_{ql}$. Hence, (24) can be simplified as

$$\frac{\alpha_{1,\mathrm{opt}}}{\alpha_{2,\mathrm{opt}}}\approx\frac{1}{\tau}. \tag{25}$$

Based on (25), this article proposes a practical control strategy to find optimal α_1 and α_2, which does not require inverter voltage and machine parameters. If we control α_1 and α_2 independently, the control structure will be complex. To this end, a new coefficient α ($0\le\alpha\le1$) is introduced and based on (25), α_1 and α_2 can be represented as

$$\begin{cases}\alpha_2=\alpha,\ \alpha_1=\alpha\frac{1}{\tau},\ \text{if}\ \ \tau>1\\ \alpha_1=\alpha,\ \alpha_2=\alpha\tau,\qquad \text{else}.\end{cases} \tag{26}$$

It is obvious that α_1 and α_2 in (26) will always satisfy (25). With (26), the control structure can be simplified. Specifically, with (26), one needs to control only α for current harmonic suppression. If there is no inverter voltage limit, α is set to zero. With inverter voltage limit, the proposed control strategy is an iterative search based method for determining the optimal α. The idea is that one can decrease α gradually until the current harmonic magnitude is not decreasing any more, and then optimal α is obtained. This is the conceptual idea. More specifically, α can be controlled as follow. Initially set α to 1, and then at time t update $\alpha_t=\alpha_{t\text{-}1}-\Delta\alpha$ if the input of the PI controller (I_i^{ref}–I_i, $i=3,4,7,8$) is zero (the harmonic magnitudes are minimized to $\alpha_{1,t\text{-}1}I_{dl,0}$ and $\alpha_{2,t\text{-}1}I_{ql,0}$), otherwise keep $\alpha_t=\alpha_{t\text{-}1}$. Here, $\Delta\alpha$ is a predefined small positive value. Practically, the input of the PI controller (I_i^{ref}–I_i) will never be zero due to measurement noise and uncertainties, and thus, "the input of the PI controller is zero" can be revised as "the input of the PI controller is smaller than a small positive value ε." Once the current harmonic magnitude is not decreasing any more, optimal α is obtained. Here, the control of α is operating at a lower sampling rate as compared with the current control in the machine drive.

Algorithm I: Control of α.

1. Set α to 1
2. At time t, **If** $\Sigma_i|I_i^{\mathrm{ref}}\text{-}I_i|<\varepsilon$, $\alpha_t=\alpha_{t\text{-}1}\text{-}\Delta\alpha$, **else** $\alpha_t=\alpha_{t\text{-}1}$
3. If $\Sigma_i|I_i^{\mathrm{ref}}\text{-}I_i|$ at t+1 is larger than $\Sigma_i|I_i^{\mathrm{ref}}\text{-}I_i|$ at t

Optimal α is α_t

TABLE I
UNDER INVERTER VOLTAGE LIMIT, THE DQ2 FRAME HARMONIC CURRENTS AND VOLTAGES USING ALGORITHM I

t=0	t=1	t=2	t
$i_{dl,0}$	(1-Δα)$i_{dl,0}$	(1-2Δα)$i_{dl,0}$	(1-tΔα)$i_{dl,0}$
$i_{ql,0}$	(1-Δα)τ$i_{ql,0}$	(1-2Δα)τ$i_{ql,0}$	(1-tΔα)τ$i_{ql,0}$
v_{dl}	Δα$i_{dl,0}$$Z_{dl}$	2Δα$i_{dl,0}$$Z_{dl}$	tΔα$i_{dl,0}$$Z_{dl}$
v_{ql}	-(1-τ+Δατ)$i_{ql,0}$$Z_{ql}$	-(1-τ+2Δατ)$i_{ql,0}$$Z_{ql}$	-(1-τ+tΔατ)$i_{ql,0}$$Z_{ql}$
$\lvert v_{dl}\rvert+\lvert v_{ql}\rvert$	2Δα$I_{dl,0}\lvert Z_{dl}\rvert+v_0$	4Δα$I_{dl,0}\lvert Z_{dl}\rvert+v_0$	2tΔα$I_{dl,0}\lvert Z_{dl}\rvert+v_0$

The control of α is summarized as in Algorithm I. At time t, the reference values in Fig. 3 can be calculated as follows. Applying transformation matrices to DQ frame currents before CHM, the obtained initial dc values are denoted as $I_{1,0},\ldots,I_{8,0}$, which is obtained from (10). Then, the references at time t can be calculated from

$$\begin{cases}I_{3,t}^{\mathrm{ref}}=0.5\left(\alpha_{1,t}(I_{3,0}+I_{7,0})+\alpha_{2,t}(I_{3,0}-I_{7,0})\right)\\ I_{4,t}^{\mathrm{ref}}=0.5\left(\alpha_{2,t}(I_{4,0}+I_{8,0})+\alpha_{1,t}(I_{4,0}-I_{8,0})\right)\\ I_{7,t}^{\mathrm{ref}}=0.5\left(\alpha_{1,t}(I_{3,0}+I_{7,0})-\alpha_{2,t}(I_{3,0}-I_{7,0})\right)\\ I_{8,t}^{\mathrm{ref}}=0.5\left(\alpha_{2,t}(I_{4,0}+I_{8,0})-\alpha_{1,t}(I_{4,0}-I_{8,0})\right).\end{cases} \tag{27}$$

Proof to (27): See the Appendix.

The proof that Algorithm I is capable of finding the optimal α is as follows. At $t=0$, DQ_2 frame current harmonics are $i_{dl,0}$ and $i_{ql,0}$. Without loss of generality, assume that the magnitude of $i_{ql,0}$ is larger than that of $i_{dl,0}$. Using Algorithm I, at $t=1$, $i_{dl,0}$ is minimized to $(1-\Delta\alpha)i_{dl,0}$ and $i_{ql,0}$ is minimized to $\tau(1-\Delta\alpha)i_{ql,0}$. According to (6) and (18), the required voltages v_{dl} and v_{ql} are $-\Delta\alpha i_{dl,0}Z_{dl}$ and $-(1-\tau+\Delta\alpha\tau)i_{ql,0}Z_{ql}$, respectively, thus $|v_{dl}|+|v_{ql}|$ is $2\Delta\alpha I_{dl,0}|Z_{dl}|+v_0$, where $v_0=(1-\tau)I_{ql,0}|Z_{ql}|$ and $Z_{dl}=Z_{ql}$. In each sampling time, the harmonic currents and voltages are listed in Table I, which shows that $|v_{dl}|+|v_{ql}|$ is increased by $2\Delta\alpha I_{dl,0}|Z_{dl}|$ in each iteration. At time t, if the inverter voltage is available, then the current harmonics can be

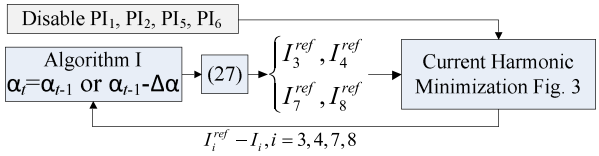

Fig. 4. Current harmonic reduction considering inverter voltage limit.

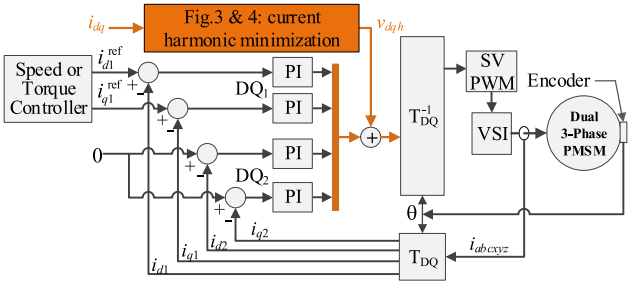

Fig. 5. Implementation of CHM in a motor drive.

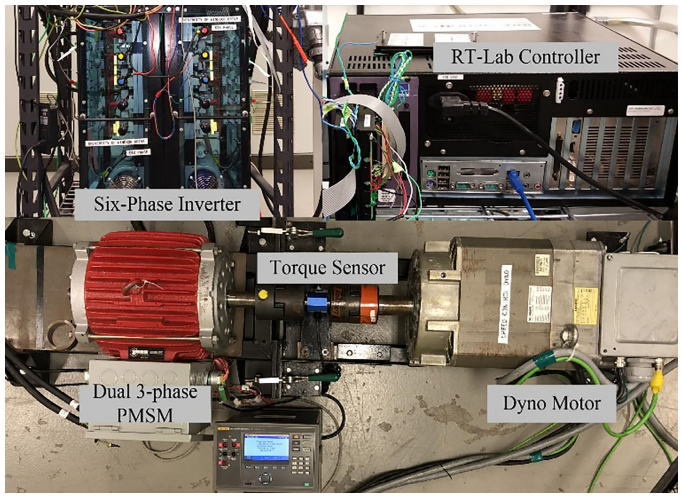

Fig. 6. Experimental setup.

TABLE II
DESIGN PARAMETERS OF THE TEST MOTOR

Rated current	15 A	NO. of slots	48
Rated torque	75 Nm	L_Δ@ I_s=15 A,γ=30°	-21 mH
Rated speed	575 rpm	Magnet flux Λ_0	0.339 Wb
Rated voltage	140 V	NO. of pole pairs	4

minimized to $(1–t\Delta\alpha)i_{dl,0}$ and $(1–\tau–t\Delta\alpha\tau)i_{ql,0}$, and $|v_{dl}|+|v_{ql}|$ is increased by $2\Delta\alpha I_{dl,0}|Z_{dl}|$. $|v_{dl}|+|v_{ql}|$ will keep increasing until it reaches the voltage limit and the harmonic current magnitude will stop decreasing. In this case, the condition in Algorithm I is satisfied and the optimal coefficient is obtained.

C. Implementation and Comparison With Existing Method

The implementation of proposed approach is summarized in Figs. 3–5. In Fig. 5, voltage harmonics are generated to be added to the voltage references for CHM, which shows that harmonic current minimization control is independent from the dc current control, and thus, the proposed approach will not affect the current control for torque production. Without inverter voltage limit, I_1^{ref} to I_8^{ref} in Fig. 3 are set to zero to minimize the current harmonics. When the inverter voltage is limited, 1st, 2nd, 5th, and 6th PI controllers are disabled in Fig. 3, and I_3^{ref}, I_4^{ref}, I_7^{ref}, and I_8^{ref} are obtained from Fig. 4 to achieve current harmonic reduction. Hence, the proposed approach is capable of current harmonic suppression with inverter voltage limit.

In [38], the method aims to minimize the current harmonics in *abcxyz* frame, in which a new transformation is developed to convert the 5th and 7th harmonics in *abcxyz* frame into the dc components and then PI controller is employed to control the dc components to zero. In implementation, T_{DQ} in Fig. 5 will be replaced with a new transformation matrix in [38]. However, the new transformation converts the DQ_2 frame dc currents into harmonic components in the new frame, which will affect the current control in the synchronous frame, although DQ_2 frame currents do not contribute to torque production. Its performance can be affected by DQ_2 frame transient currents. On the other hand, the proposed approach minimizes the current harmonics in the synchronous frame and does not affect the dc current control in both DQ_1 and DQ_2 frames. Therefore, the performance will be better than that in [38] during the transient conditions, which will be validated with experiments. More importantly, the proposed approach considers inverter voltage limit with comprehensive theoretical analyses.

IV. EXPERIMENTAL INVESTIGATIONS

The proposed CHM approach is tested on a laboratory dual three-phase PMSM drive, as shown in Fig. 6, and the design parameters are listed in Table II. Three tests are conducted to validate proposed approach, in which the inverter voltage is sufficient in Tests 1 and 2 and it is limited in Test 3. Moreover, the proposed approach is compared with the method in [38] under both steady-state and transient conditions in Test 2 to demonstrate the performance improvement.

Test 1 is conducted to validate the proposed approach under various load conditions. The original DQ frame currents of the test motor under various loads are shown in Fig. 7. Here, 12th and 6th harmonics are dominant. Fig. 7 presents the magnitudes of the 12th and 6th current harmonics in DQ_1 and DQ_2 frames. In Fig. 7, the test motor operates at a speed of 100 r/min. It can be observed from Fig. 7 that 6th current harmonic has a much larger magnitude than 12th one; as the stator current increases, the magnitude of 6th harmonic increases as well. The proposed approach is then applied to minimize the current harmonics in DQ_1 and DQ_2 frames. Fig. 8 presents the minimization results under every load condition in Fig. 7. As shown in Fig. 8, the current harmonics have been reduced significantly. For instance, under the stator current of 5 A, the 12th harmonics in DQ_1 frame and 6th harmonics in DQ_2 frame have magnitudes of 31, 62, 265, and 306 mA, respectively; however, after minimization, according to Fig. 8, they are 5, 3, 2, and 2 mA, respectively. Compared with Fig. 7, 12th harmonic magnitudes in DQ_1 frame and 6th

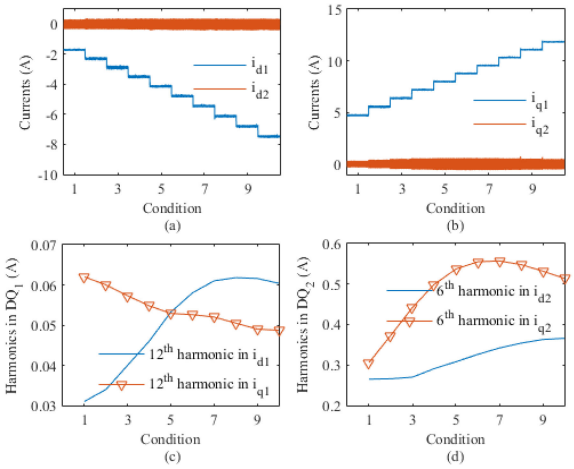

Fig. 7. DQ frame currents under various load conditions before CHM in Test 1. (a) D_1D_2 frame. (b) Q_1Q_2 frame. (c) Twelfth current harmonic magnitudes. (d) Sixth current harmonic magnitudes. The harmonic magnitude in DQ_2 frame is much larger than that in DQ_1 frame.

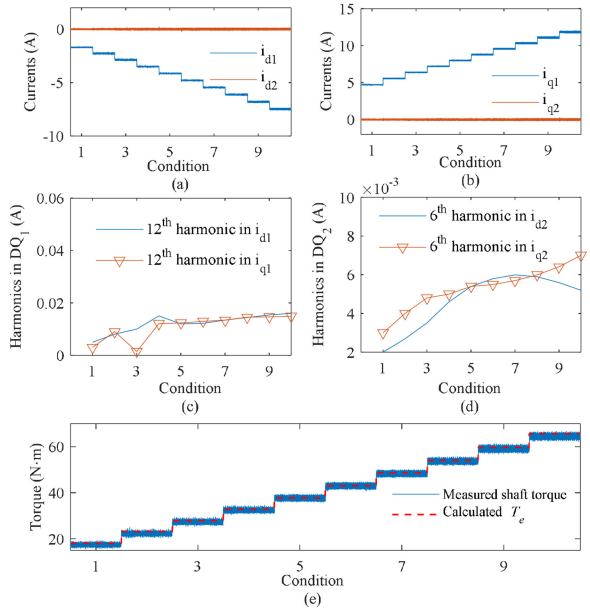

Fig. 8. DQ frame currents after CHM in Test 1. (a) D_1D_2 frame. (b) Q_1Q_2 frame. (c) Twelfth current harmonic magnitudes. (d) Sixth current harmonic magnitudes. (e) Torque information.

harmonic magnitudes in DQ_2 frame have been minimized to near zero, as shown in Fig. 8(c) and (d).

On the other hand, Fig. 9 presents phase a and x current comparison without and with the proposed approach under the stator current of 5 A. In Fig. 9, there are obvious harmonics in the phase currents due to motor and drive nonlinearities, but the phase currents are close to sinusoidal waveforms after CHM. The results before and after minimization at the rated current are presented in Fig. 10 and the current harmonic magnitudes are listed in Table III. In this test, the DQ_1 frame currents are set to –7.5 and 13 A, respectively. It can be seen from Table III that the proposed approach is able to minimize the current harmonic

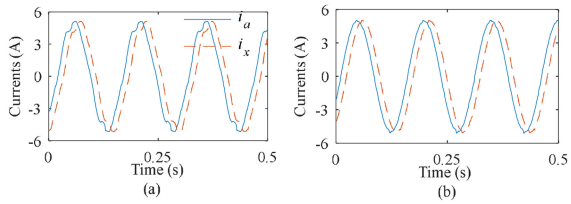

Fig. 9. Phase a and x currents. (a) Before minimization. (b) After minimization. Phase current is close to sinusoidal after CHM.

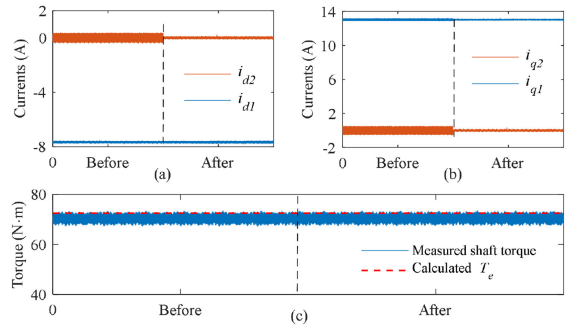

Fig. 10. DQ frame currents and torque before and after CHM at rated current. (a) D_1D_2 frame. (b) Q_1Q_2 frame. (c) Torque.

TABLE III
MAGNITUDES OF THE CURRENT HARMONICS IN DQ FRAME BEFORE AND AFTER MINIMIZATION AT RATED CURRENT

	Magnitude Before Minimization (A)	Magnitude After Minimization (A)
D_1 Frame	0.06	0.014
Q_1 Frame	0.09	0.011
D_2 Frame	0.36	0.007
Q_2 Frame	0.55	0.006

effectively under the rated current. On the other hand, the torque waveforms and the calculated torque using (2) are presented in Figs. 8(e) and 10(c), in which the inductance values used in the calculation are obtained from offline inductance maps. Here, the calculated electromagnetic torque is slightly larger than the measured shaft torque, which is mainly due to the mechanical loss. Figs. 8(e) and 10(c) demonstrate that the proposed approach will not affect the torque control because the control of current harmonics will not affect the dc current control.

In Test 2, the proposed approach is evaluated under the torque transient condition at a higher speed of 300 r/min. In this test, the stator current increases from 5 to 14 A. Fig. 11 presents the DQ frame currents before and after minimization by using the proposed approach as well as the compared method in [38]. Under transient condition, current harmonics will increase without minimization, for instance, the 6th harmonic magnitude can increase up to 1.1 A. In Fig. 11, both the proposed and compared methods can effectively minimize the current harmonics in DQ frame currents under both steady-state and transient conditions. Fig. 12 presents the comparison of the harmonic magnitudes during minimization. As can be seen from Fig. 12, when the stator current is 5 A, the harmonic magnitudes of i_{d1}, i_{q1}, i_{d2}, and i_{q2} are 130, 170, 720, and 790 mA, respectively;

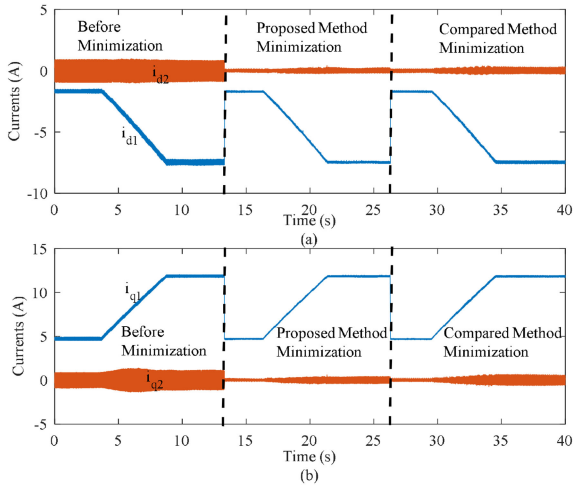

Fig. 11. Comparison before and after CHM in Test 2. (a) D_1D_2 frame currents. (b) Q_1Q_2 frame currents.

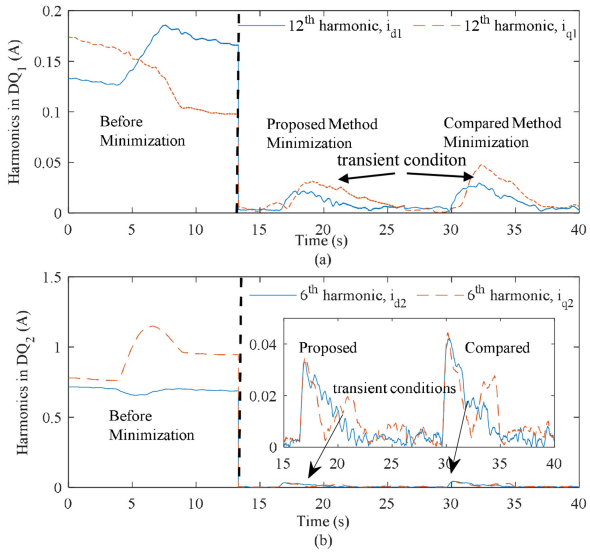

Fig. 12. Comparison of the current harmonic magnitudes under the transient condition before and after minimization in Test 2, where the proposed approach achieves a better performance during the transient condition.

they are, respectively, minimized to 3, 5, 3, and 4 mA in the proposed approach; and they are, respectively, minimized to 4, 4, 6, and 7 mA in the compared method. In Figs. 11 and 12, both the proposed and compared approaches can minimize the magnitudes of the 12th and 6th current harmonics to near zero.

However, during the transient condition, the proposed approach performs better than the compared method, as shown in Fig. 12. For instance, the peak magnitudes during the transient in Fig. 12 are 20, 30, 32, and 35 mA in the proposed approach; and they are 29, 48, 42, and 44 mA in the compared method. This indicates that the proposed approach can achieve a low current harmonic and, thus, better performance during the transient. The reason is discussed in Section III-C. It should be noted that the same PI coefficients are utilized in both the proposed and compared methods to avoid the influence from the PI controllers during the comparison. Moreover, under limited voltage, current

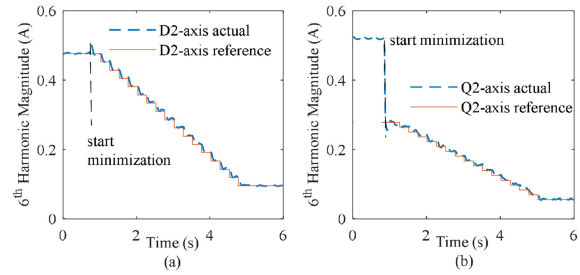

Fig. 13. DQ_2 frame current harmonic magnitudes during steady state in Test 3, where inverter voltage limit is imposed. (a) D_2 frame. (b) Q_2 frame.

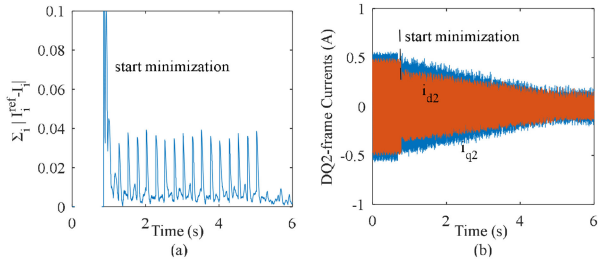

Fig. 14. Minimization results with inverter voltage limit under steady-state condition in Test 3. (a) Input to control α in Fig. 4. (b) DQ_2 frame currents.

harmonics cannot be minimized to zero, but the compared method will keep increasing the voltages until current harmonics are minimized to zero. However, the inverter is unable to deliver the required voltages, which will affect the reference voltages used for torque production. Hence, with limited voltage, the compared method is not effective and might affect the torque control, so the comparison is conducted with sufficient voltage.

In Test 3, it is assumed that the inverter voltage is limited, so this test considers to reduce DQ_2 frame current harmonics. Here, inverter voltage limit is achieved by changing the dc-link voltage, in which the available voltage can be calculated from (16). In the first test, the motor is operating at 500 r/min and the load torque is 40 N·m. Fig. 13 presents the initial DQ_2 frame 6th current harmonic magnitudes, which are 0.47 and 0.52 A, respectively, so the coefficients are calculated using the first equation in (26). The coefficient α is initially set to 1 and then gradually reduced based on the current error defined in Algorithm I. In Algorithm I, $\Delta\alpha$ is set to 0.05, which means that α is reduced by 0.05 every time when the condition is satisfied. During the minimization, the error $\Sigma_i|\, I_i^{\text{ref}} - I_i|$ is shown in Fig. 14(a), the calculated reference current magnitudes are shown in Fig. 13, and the actual DQ_2 frame currents are shown in Fig. 14(b). The actual magnitudes of 6th harmonics are compared in Fig. 13(a) and (b). From Fig. 13, when the actual current harmonics are minimized to the reference values, the reference values will be decreased until the current harmonics cannot be reduced any more, and the optimal references are obtained. The reference voltages are presented in Fig. 15. In this test, DQ_1 frame voltage dc value is about 104 V, as shown in Fig. 15(a), and the dc-link voltage is set so that the available inverter voltage is about 110 V. As shown in Fig. 15(b), the harmonic voltage magnitude will increase gradually to 9.4 and 7.8 V, respectively, and the current

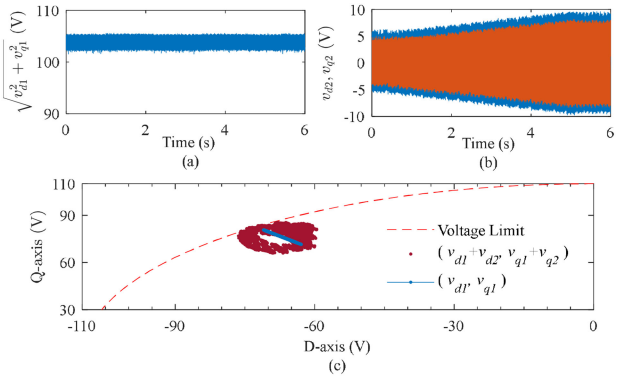

Fig. 15. DQ frame reference voltages during CHM in Test 3. (a) DQ_1 frame. (b) Harmonic voltage for DQ_2 frame. (c) Voltages in DQ frame.

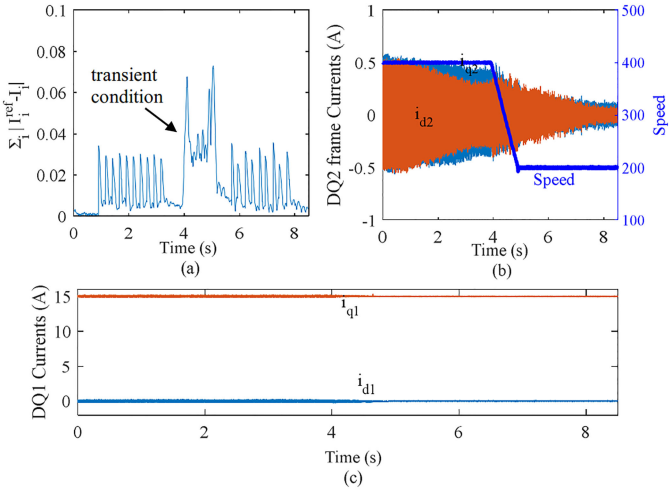

Fig. 16. Minimization results with inverter voltage limit under transient condition in Test 3. (a) Input to control α. (b) DQ_2 frame currents and speed. (c) DQ_1 frame currents.

harmonic magnitudes are decreasing gradually. In this test, the voltage limit is represented by the dash line in Fig. 15(c), whereas the DQ_1 frame voltages are the solid line, which is within the voltage limit. The harmonic voltages are added into DQ_2 frame to reduce the current harmonics and the total DQ frame voltages in Fig. 15(c) are also within the inverter voltage limit. Due to voltage limit, the 6th current harmonic is not minimized to zero.

In the second test, the proposed approach is applied to the case of speed transient condition with inverter voltage limit and the speed decreases from 400 to 200 r/min during CHM, as shown in Fig. 16. $\Delta\alpha$ is set to be the same as the first test. In this test, $\Sigma_i|\, I_i^{\text{ref}}\text{–}I_i|$ is presented in Fig. 16(a), the actual DQ_2 frame currents and motor speed are shown in Fig. 16(b), and DQ_1 frame currents are controlled to 0 and 15 A, as shown in Fig. 16(c). The calculated reference magnitudes for DQ_2 frame currents are shown in Fig. 17. It can be seen from Figs. 16(a) and 17 that under the speed transient, the magnitude of the current harmonics will slightly increase, which leads to the increase of $\Sigma_i|\, I_i^{\text{ref}}\text{–}I_i|$. Therefore, although more voltage will be available after the speed is reduced, the reference magnitude (coefficient α) is not

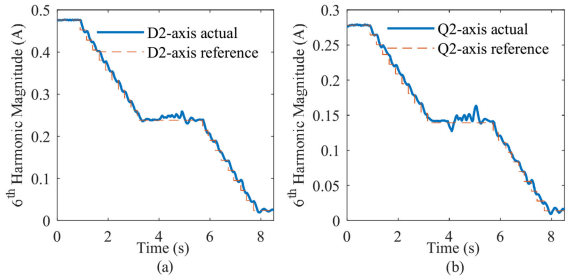

Fig. 17. DQ_2 frame current harmonic magnitudes during transient condition in Test 3, where inverter voltage limit is imposed. (a) D_2 frame. (b) Q_2 frame.

decreasing, as the condition in Algorithm I is not satisfied, so the reference magnitude is kept the same during the transient, that is, $\alpha_t = \alpha_{t\text{-}1}$ for $\Sigma_i|\, I_i^{\text{ref}}\text{–}I_i| > \varepsilon$ during the speed transient condition. Therefore, during the transient, the magnitude of 6th current harmonics is kept to be 0.24 and 0.14 A, as shown in Fig. 17; after the speed is reduced to 200 r/min, the current harmonics are further reduced. These results demonstrate that the proposed approach is capable of current harmonic suppression under both steady-state and transient conditions with limited inverter voltage.

V. Conclusion

An efficient DRF-based CHM approach is developed for dual three-phase PMSMs, which is effective under the constraint of inverter voltage limit. The derived current harmonic model indicates that the dominant harmonics occupy most of the current harmonics. Hence, the proposed approach converts the dominant current harmonics in the synchronous frame into the dc components by using DRFs and minimizes dc components by using PI controllers. Under inverter voltage limit, optimal solution for current harmonic reduction is theoretically derived and a practical iterative search based control strategy is developed to eliminate the need of inverter voltage and machine parameters. Test results demonstrate that the proposed approach is effective for CHM under various operating conditions and performs better than the compared method especially under transient conditions. With limited voltage, this article assumes that the voltage is used to reduce DQ_2 frame current harmonics. When the voltage is enough to minimize DQ_2 frame current harmonics but limited to reduce DQ_1 frame current harmonics, I_3^{ref}, I_4^{ref}, I_7^{ref}, and I_8^{ref} will be set to zero, and I_1^{ef}, I_2^{ref}, I_5^{ref}, and I_6^{ref} can be obtained from Fig. 4, in which the parameters should be updated accordingly.

Appendix

According to Hu *et al.* [30] and Kallio *et al.* [32], the self-inductance of phase *i* can be denoted as

$$L_i = L_{sl} + L_{s0} + L_{s2}\cos(2\theta_i). \tag{28}$$

The mutual inductance between phases *i* and *j* in the same set of windings can be denoted as

$$M_{ij} = M_{m0,1}\cos(\theta_i - \theta_j) + M_{s2,1}\cos(\theta_i + \theta_j). \tag{29}$$

The mutual inductance between phases *i* and *j* in different set of windings can be denoted as

$$M_{ij} = M_{m0,2}\cos(\theta_i - \theta_j) + M_{m2,2}\cos(\theta_i + \theta_j) \tag{30}$$

Here L_{sl} is the phase leakage inductance; and L_{s0}, $M_{s0,1}$, and $M_{s0,2}$ are the dc values; L_{s2}, $M_{s2,1}$, and $M_{s2,2}$ are the second-harmonic coefficients. The detailed definitions of these coefficients can be found in [30] and [32]. When the transformation is applied to the inductance matrix, DQ frame inductances can be derived as

$$\begin{cases} L_{d1} = L_{sl} + 3L_d, L_{q1} = L_{sl} + 3L_q \\ L_{d2} = L_{q2} = L_{sl} \end{cases}$$
$$\text{with} \begin{cases} L_d = L_{s0} + L_{s2} \\ L_q = L_{s0} - L_{s2} \end{cases} \tag{31}$$

where L_{d1} and L_{q1} are DQ_1 frame inductances; and L_{d2} and L_{q2} are DQ_2 frame inductances and are equal to the leakage inductance, which also confirms with the results in [19].

Proof to Theorem 1: Substituting $I_1 = I_2 = I_5 = I_6 = 0$ into (10) yields

$$\begin{cases} I_{dk}\cos\phi_{dk} + I_{qk}\sin\phi_{qk} = 0, \ I_{dk}\sin\phi_{dk} - I_{qk}\cos\phi_{qk} = 0 \\ I_{dk}\cos\phi_{dk} - I_{qk}\sin\phi_{qk} = 0, \ I_{dk}\sin\phi_{dk} + I_{qk}\cos\phi_{qk} = 0. \end{cases} \tag{32}$$

With (32), we can derive $I_{dk} = I_{qk} = 0$. Similarly, substituting $I_3 = I_4 = I_7 = I_8 = 0$ into (10), we can derive $I_{dl} = I_{ql} = 0$.

Proof to (27): Substituting $I_{1,0}, \ldots, I_{8,0}$ into (10), we have

$$\begin{cases} I_{dl}\cos\phi_{dl} = I_{3,0} + I_{7,0}, \ I_{ql}\sin\phi_{ql} = I_{3,0} - I_{7,0} \\ I_{dl}\sin\phi_{dl} = I_{4,0} - I_{8,0}, \ I_{ql}\cos\phi_{ql} = I_{4,0} + I_{8,0}. \end{cases} \tag{33}$$

At time *t*, the current harmonics are reduced to $\alpha_{1,t} i_{dl,0}$ and $\alpha_{2,t} i_{ql,0}$, that is, the reference currents are $\alpha_{1,t} i_{dl,0}$ and $\alpha_{2,t} i_{ql,0}$. Substituting $\alpha_{1,t} i_{dl,0}$, $\alpha_{2,t} i_{ql,0}$, and (33) into (10), we have (27).

REFERENCES

[1] Y. Hu, H. Shoudao, X. Wu, and X. Li, "Control of dual three-phase permanent magnet synchronous machine based on five-leg inverter," *IEEE Trans. Power Electron.*, vol. 34, no. 11, pp. 11071–11079, Nov. 2019.

[2] S. Kwon and J. Ha, "Fault-tolerant operation under single-phase open in mono inverter dual parallel SMPMSM with single shaft," *IEEE Trans. Power. Electron.*, vol. 34, no. 12, pp. 12064–12079, Dec. 2019.

[3] X. Wang, Z. Wang, Z. Xu, M. Cheng, W. Wang, and Y. Hu, "Comprehensive diagnosis and tolerance strategies for electrical faults and sensor faults in dual three-phase PMSM drives," *IEEE Trans. Power Electron.*, vol. 34, no. 7, pp. 6669–6684, Jul. 2019.

[4] H. M. Eldeeb, A. S. Abdel-Khalik, and C. M. Hackl, "Postfault full torque–speed exploitation of dual three-phase IPMSM drives," *IEEE Trans. Ind. Electron.*, vol. 66, no. 9, pp. 6746–6756, Sep. 2019.

[5] G. Feng, C. Lai, M. Kelly, and N. C. Kar, "Dual three-phase PMSM torque modelling and maximum torque per peak current control through optimized harmonic current injection," *IEEE Trans. Ind. Electron.*, vol. 66, no. 5, pp. 3356–3368, May 2019.

[6] Y. Hu, Z. Q. Zhu, and K. Liu, "Current control for dual three-phase permanent magnet synchronous motors accounting for current unbalance and harmonics," *IEEE J. Emerg. Sel. Topics Power Electron.*, vol. 2, no. 2, pp. 272–284, Jun. 2014.

[7] G. Liu, B. Chen, K. Wang, and X. Song, "Selective current harmonic suppression for high-speed PMSM based on high-precision harmonic detection method," *IEEE Trans. Ind. Informat.*, vol. 15, no. 6, pp. 3457–3468, Jun. 2019.

[8] W. Zhang, Y. Xu, H. Huang, and J. Zou, "Vibration reduction for dual-branch three-phase permanent magnet synchronous motor with carrier phase-shift technique," *IEEE Trans. Power Electron.*, vol. 35, no. 1, pp. 607–618, Jan. 2020.

[9] A. G. Yepes, J. Doval-Gandoy, F. Baneira, D. Pérez-Estévez, and O. López, "Current harmonic compensation for n-phase machines with asymmetrical winding arrangement and different neutral configurations," *IEEE Trans. Ind. Appl.*, vol. 53, no. 6, pp. 5426–5439, Nov./Dec. 2017.

[10] K. Liu, J. Feng, S. Guo, L. Xiao, and Z. Q. Zhu, "Identification of flux linkage map of permanent magnet synchronous machines under uncertain circuit resistance and inverter nonlinearity," *IEEE Trans. Ind. Informat.*, vol. 14, no. 2, pp. 556–568, Feb. 2018.

[11] J. Yang, W. Chen, S. Li, L. Guo, and Y. Yan, "Disturbance/uncertainty estimation and attenuation techniques in PMSM drives—A survey," *IEEE Trans. Ind. Electron.*, vol. 64, no. 4, pp. 3273–3285, Apr. 2017.

[12] J. Lara, J. Xu, and A. Chandra, "Effects of rotor position error in the performance of field-oriented-controlled PMSM drives for electric vehicle traction applications," *IEEE Trans. Ind. Electron.*, vol. 63, no. 8, pp. 4738–4751, Aug. 2016.

[13] W. Liang, W. Fei, and P. C. Luk, "An improved sideband current harmonic model of interior PMSM drive by considering magnetic saturation and cross-coupling effects," *IEEE Trans. Ind. Electron.*, vol. 63, no. 7, pp. 4097–4104, Jul. 2016.

[14] N. Y. A. Qamar and C. J. Hatziadoniu, "Cancelation of torque ripples in PMSM via a novel minimal parameter harmonic flux estimator," *IEEE Trans. Power Electron.*, vol. 34, no. 3, pp. 2553–2562, Mar. 2019.

[15] Z. Tang and B. Akin, "Suppression of dead-time distortion through revised repetitive controller in PMSM drives," *IEEE Trans. Energy Convers.*, vol. 32, no. 3, pp. 918–930, Sep. 2017.

[16] F. Lin, S. Zuo, W. Deng, and S. Wu, "Modeling and analysis of electromagnetic force, vibration, and noise in permanent-magnet synchronous motor considering current harmonics," *IEEE Trans. Ind. Electron.*, vol. 63, no. 12, pp. 7455–7466, Dec. 2016.

[17] Z. Zhang, X. Ge, Z. Tian, X. Zhang, Q. Tang, and X. Feng, "A PWM for minimum current harmonic distortion in metro traction PMSM with saliency ratio and load angle constrains," *IEEE Trans. Power Electron.*, vol. 33, no. 5, pp. 4498–4511, May 2018.

[18] A. G. Yepes, J. Malvar, A. Vidal, O. López, and J. Doval-Gandoy, "Current harmonics compensation based on multiresonant control in synchronous frames for symmetrical n-phase machines," *IEEE Trans. Ind. Electron.*, vol. 62, no. 5, pp. 2708–2720, May 2015.

[19] Z. Wu, W. Gu, K. Lu, Y. Zhu, and J. Guan, "Current harmonic suppression algorithm for asymmetric dual three-phase PMSM," *Appl. Sci.*, vol. 10, 2020, Art. no. 954.

[20] K. Liu and Z. Zhu, "Position offset-based parameter estimation for permanent magnet synchronous machines under variable speed control," *IEEE Trans. Power Electron.*, vol. 30, no. 6, pp. 3438–3446, Jun. 2015.

[21] D. Li, Y. Iwaji, Y. Notohara, and K. Kishita, "Harmonic current cancellation method for PMSM drive system using resonant controllers," in *Proc. Int. Power Electron. Conf.*, 2018, pp. 1301–1307.

[22] Z. Ruan, W. Song, and Y. Yan, "Current harmonic suppression for dual three-phase permanent magnet synchronous motor drives," *IEEE Access*, vol. 7, pp. 143888–143898, 2019.

[23] C. Xia, B. Ji, and Y. Yan, "Smooth speed control for low-speed high-torque permanent-magnet synchronous motor using proportional–integral–resonant controller," *IEEE Trans. Ind. Electron.*, vol. 62, no. 4, pp. 2123–2134, Apr. 2015.

[24] A. Abosh, Z. Zhu, and Y. Ren, "Reduction of torque and flux ripples in space vector modulation-based direct torque control of asymmetric permanent magnet synchronous machine," *IEEE Trans. Power Electron.*, vol. 32, no. 4, pp. 2976–2986, Apr. 2017.

[25] Y. Luo and C. Liu, "Elimination of harmonic currents using a reference voltage vector based-model predictive control for a six-phase PMSM motor," *IEEE Trans. Power Electron.*, vol. 34, no. 7, pp. 6960–6972, Jul. 2019.

[26] Y. Luo and C. Liu, "A simplified model predictive control for a dual three-phase PMSM with reduced harmonic currents," *IEEE Trans. Ind. Electron.*, vol. 65, no. 11, pp. 9079–9089, Nov. 2018.

[27] Y. Ren and Z. Q. Zhu, "Reduction of both harmonic current and torque ripple for dual three-phase permanent-magnet synchronous machine using modified switching-table-based direct torque control," *IEEE Trans. Ind. Electron.*, vol. 62, no. 11, pp. 6671–6683, Nov. 2015.

[28] J. Hwang and H. Wei, "The current harmonics elimination control strategy for six-leg three-phase permanent magnet synchronous motor drives," *IEEE Trans. Power Electron.*, vol. 29, no. 6, pp. 3032–3040, Jun. 2014.

[29] L. Wang, Z. Q. Zhu, H. Bin, and L. M. Gong, "Current harmonics suppression strategy for PMSM with non-sinusoidal back-EMF based on adaptive linear neuron method," *IEEE Trans. Ind. Electron.*, vol. 67, no. 11, pp. 9164–9173, Nov. 2020.
[30] Y. Hu, Z. Q. Zhu, and M. Odavic, "Comparison of two-individual current control and vector space decomposition control for dual three-phase PMSM," *IEEE Trans. Ind. Appl.*, vol. 53, no. 5, pp. 4483–4492, Sep./Oct. 2017.
[31] H. Eldeeb, A. S. Abdel-Khalik, and C. Hackl, "Dynamic modelling of dual three-phase IPMSM drives with different neutral configurations," *IEEE Trans. Ind. Electron.*, vol. 66, no. 1, pp. 141–151, Jan. 2019.
[32] S. Kallio, M. Andriollo, A. Tortella, and J. Karttunen, "Decoupled d-q model of double-star interior-permanent-magnet synchronous machines," *IEEE Trans. Ind. Electron.*, vol. 60, no. 6, pp. 2486–2494, Jun. 2013.
[33] J. Karttunen, S. Kallio, J. Honkanen, P. Peltoniemi, and P. Silventoinen, "Partial current harmonic compensation in dual three-phase PMSMs considering the limited available voltage," *IEEE Trans. Ind. Electron.*, vol. 64, no. 2, pp. 1038–1048, Feb. 2017.
[34] G. Feng, C. Lai, J. Tian, and N. C. Kar, "Multiple reference frame based torque ripple minimization for PMSM drive under both steady-state and transient conditions," *IEEE Trans. Power Electron.*, vol. 34, no. 7, pp. 6685–6696, Jul. 2019.
[35] D. Reigosa, D. Fernandez, H. Yoshida, T. Kato, and F. Briz, "Permanent-magnet temperature estimation in PMSMs using pulsating high-frequency current injection," *IEEE Trans. Ind. Appl.*, vol. 51, no. 4, pp. 3159–3168, Jul. 2015.
[36] D. Reigosa, D. Fernandez, T. Tanimoto, T. Kato, and F. Briz, "Comparative analysis of BEMF and pulsating high-frequency current injection methods for PM temperature estimation in PMSMs," *IEEE Trans. Power Electron.*, vol. 32, no. 5, pp. 3691–3699, May 2017.
[37] A. Salem and M. Narimani, "A review on multiphase drives for automotive traction applications," *IEEE Trans. Transp. Electrific.*, vol. 5, no. 4, pp. 1329–1348, Dec. 2019.
[38] F. Yuan, S. Huang, and W. Long, "Techniques to restrain harmonics of six-phase permanent magnet synchronous motors," *Trans. China Electrotech. Soc.*, vol. 26, no. 9, pp. 31–36, 2011.

Guodong Feng (Senior Member, IEEE) received the B.S. and Ph.D. degrees in engineering from Sun Yat-sen University, Guangzhou, China, in 2010 and 2015, respectively.

From 2015 to 2019, he was a Postdoctoral Fellow with the University of Windsor, Windsor, ON, Canada. He is currently an Associate Professor with the School of Intelligent Systems Engineering, Sun Yat-sen University. His research interests include advanced signal processing, optimization, and electrical machines and drives.

Chunyan Lai (Senior Member, IEEE) received the B.S. degree in engineering from Sun Yat-sen University, Guangzhou, China, in 2010, and the Ph.D. degree in electrical and computer engineering from the University of Windsor, Windsor, ON, Canada, in 2017.

She was a Postdoctoral Fellow with the University of Windsor, from 2017 to 2018. She is currently an Assistant Professor with the Department of Electrical and Computer Engineering, Concordia University, Montreal, QC, Canada. Her research areas include electric machine drives and controls and other power electronics related applications, such as renewable energy.

Wenlong Li (Senior Member, IEEE) received the B.Eng. degree from Sichuan University, Chengdu, China, in 2005, the M.Eng. degree from the University of Science and Technology of China, Hefei, China, in 2008, and the Ph.D. degree from The University of Hong Kong, Hong Kong, in 2012.

He is currently a Visiting Scholar with the University of Windsor, Windsor, ON, Canada. His research interests include electrical machine design, analysis, and applications. He has also authored/coauthored more than 70 peer-viewed technical papers and three invited book chapters in these areas.

Ze Li (Graduate Student Member, IEEE) received the B.Eng. and M.Eng. degrees from the Xi'an University of Architecture and Technology, Xi'an, China, in 2012 and 2015, respectively. He is currently working toward the Ph.D. degree with the University of Windsor, Windsor, ON, Canada.

He was a Testing Engineer with D&V Electronics Company, Ltd., Woodbridge, ON, Canada, in 2017. His research interests include modeling and control of electric power converters and electrical machines, and machine parameter identification, testing, and performance analysis.

Narayan C. Kar (Senior Member, IEEE) received the B.S. degree from the Bangladesh University of Engineering and Technology, Dhaka, Bangladesh, in 1992, and the M.S. and Ph.D. degrees from the Kitami Institute of Technology, Hokkaido, Japan, in 1997 and 2000, respectively, all in electrical engineering.

He is currently a Professor with the Department of Electrical and Computer Engineering, University of Windsor, Windsor, ON, Canada, where he also holds the Canada Research Chair position. His current research interests include the analysis, design, and control of electrical machines for electrified vehicle applications.